Time accurate numerical cavitation erosion prediction of multiphase flow through a venturi

Batuhan Aktas[1,*], Dmitriy Ponkratov[2]

[1] Naval Architecture, Ocean & Marine Engineering, University of Strathclyde, Glasgow, UK

[2]Technical Investigation Department (TID), Lloyd's Register, London, UK

ABSTRACT

Cavitation erosion affects the efficient operation of the vessel's propeller, leading to increased costs of operation and maintenance. Traditionally, erosion is predicted using dedicated cavitation tests with utilization of soft paint application or materials as erosive sensors. However, even with materials that are most susceptible to erosion, such tests constitute significant amount of time. It is well-known that cavitation erosion occurs with the impact of high velocity liquid jets generated by the imploding bubbles, also called water hammer effect, and induced shock waves over time. However, it is both not a viable approach to simulate the complete duration of an experiment using numerical methods and extremely expensive in terms of computational time. Therefore, it is a common simplification to assume cavitation events to be repetitive for numerical simulations and based on this assumption there has been a plethora of studies utilizing the numerical simulations for cavitation erosion prediction. Whilst these simulations utilize instantaneous erosive power indicators for cavitation erosion estimation, an approach that takes into account of the summation/accumulation of the erosive intensity over time for precise erosion threshold determination is non-existent.

Within this framework this study presents a time accurate numerical cavitation erosion prediction based on the intriguing experimental study conducted by Petkovšek & Dular (2013) that achieved visual cavitation erosion within 1.5 seconds. In addition to the well-known erosive indicators such as Erosive Power Function (Eskilsson & Bensow, 2015), Gray Level Method (Dular et al., 2006) and Intensity Function Method (van Terwisga et al., 2009), in house functions developed by Lloyds Register (LR) Technical Investigation Department (TID) (Ponkratov, 2015; Ponkratov & Caldas, 2015) are used to compare against the experimental results. Comparisons both aided the determination of a time accurate threshold and utilized as an evaluation case for each erosive indicator.

Keywords

Cavitation, Erosion, Erosive Indicators, Multiphase Flow.

1 INTRODUCTION

Cavitation is a detrimental phenomenon for marine vehicles particularly in the field of propulsion. It manifests itself with undesirable effects to vessel's operation by induced noise and vibration, deterioration of propeller performance and erosion. Amongst aforementioned undesirable consequences, cavitation erosion is considered to be most catastrophic as it can lead to increased noise and vibration, loss of propeller performance as well as high maintenance costs.

Thus, prediction of cavitation erosion at an early design stage carries great importance. Current state of the art mainly relies on experimental investigations for the determination of erosive cavitation presence. These tests involve covering the blade foil sections with erosion prone material (Dular et al., 2006) or coating the propeller with soft paints that present pitting over significantly shorter time in comparison to full-scale operating conditions that cause cavitation erosion (Mantzaris et al., 2015). Nevertheless, carrying out such tests are mostly based on decades of experimental experience of renowned testing facilities and constitute significant amount of time and resources to carry out.

For similar cavitation problems, such as noise, vibration and performance breakdown, it is generally possible to predict with reasonable accuracy using statistical, empirical or semi-empirical methods. However, it is rather impossible for cavitation erosion since it mainly occurs with the impact of high velocity liquid jets generated by the imploding bubbles and an accumulative process of consequent impacts over time (Bark & Bensow, 2014). Moreover, to further complicate the phenomena, properties of the collapse of cavitation such as location, velocity, area/volume, bubble shape, micro jet occurrence are all influential over the erosive potential of a cavitation (Bark et al., 2004).

The lack of existence of such crucial, quick means of predictive tools resulted in development of more

[*] *Corresponding Author*

E-mail address:Batuhan.aktas@strath.ac.uk

complicated erosive indicators. These erosive indicators are derived from multiphase flow simulations using high fidelity Computational Fluid Dynamics (CFD) methods such as Reynolds Averaged Navier Stokes equations solvers (RANS), Large Eddy Simulation (LES) and Detached Eddy Simulations (DES) (SIEMENS PLM Software, 2016). Such sophisticated computational simulations provide enhanced insight to the flow properties, particularly in terms of cavitation dynamics.

With the detailed information produced by the CFD simulations, development of erosive indicators became possible. Two commonly used methods include Intensity Function Method (IFM) (van Terwisga et al., 2009) and Gray Level Method (GLM) (Dular et al., 2006). The former one is based on the time derivative of the local pressure ($\partial p/\partial t$) and the latter is calculated using the time derivative of cavitation volume ($\partial V_v/\partial t$). Furthermore, an additional erosive indicator, named Erosive Power (Eskilsson & Bensow, 2015), is used, that is developed by Usta et al. (2017) based on a combination IFM and GLM methods and given by Equation 1. The pressure derivative part of the term is multiplied by cavitation volume and cavitation volume derivative is multiplied by the difference of local pressure and vapour pressure. This inherently means that, indicator predicts no erosion to not happen when cavitation does not exist. Moreover, in the phase where cavitation volume is rising local pressure will be lower than vapour pressure hence the first term will be negative also agreeing with general conception of erosion occurrence during the collapse of cavitation.

$$I_{EPM} = (P - P_v)\left(\frac{dV_V}{dt}\right) + V_V\left(\frac{dP}{dt}\right) \qquad (1)$$

where: P is the local pressure, P_v is the vapour pressure for given temperature and V_V is the cavitation volume.

Although based on such sophisticated software and derived using complex cavitation dynamics, it is computationally impossible to simulate the whole duration of a cavitation erosion experiment. Thus, it is generally assumed by CFD simulations that the cavitation events will be repetitive over the time. However, with regards to cavitation, particularly for erosive events, this may not be the case. In this respect, time independent simulations mainly have an impact on the determination of the erosive indicator thresholds for the previously discussed predictors.

Within this framework, this study aims to simulate a multiphase flow through a venturi section that experiences cavitation erosion within 1.5 seconds. Time accurate prediction of the cavitating flow and comparisons against the experimental findings are utilized for the determination of accurate erosive indicator thresholds

Following this introduction, experimental study that is being replicated is presented in Section 2. Section 3, explains the numerical setup. Section 4 discusses and compares the numerical findings against the experimental results. Finally, Section 5 outlines the drawn conclusions.

2 EXPERIMENTAL SETUP

Experiments that have achieved visual cavitation erosion damage are performed using a closed circuit water channel with a venturi section as shown by Figure 1. Details of the experimental setup and facility are provided by (Jian et al., 2015; Petkovšek & Dular, 2013).

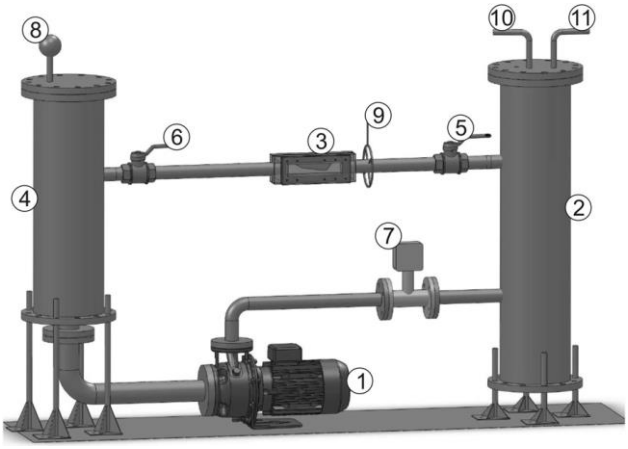

Figure 1 The experimental setup: (1) Pump, (2) upstream tank, (3) test section, (4) downstream tank, (5) and 6) valves, (7) electromagnetic flow meter, (8) thermocouple (9) pressure sensor, (10) compressor and (11) vacuum pump.

Water is circulated through the channel with the use of a 4.5kW pump which also sets the flow rate through the venturi (measurement) section. The setup utilizes an upstream tank for pressure regulation via air compressor and vacuum pump. The system temperature is regulated using the downstream tank in which a cold tap water loop is circulated through to cool down the channel water.

The flow rate of the system is measured after the circulating pump using an electromagnetic flow meter and water quality is monitored by using a Van-Slyke apparatus.

The cavitation test case was conducted while the system pressure was set to 454000 Pa with 24.7 m/s velocity through the venture throat (Figure 2) corresponding to cavitation number of 1.48. The experimental condition was achieved by initially setting the pressure and ramping up the flow velocity. It is reported that aimed conditions were reached within 0.05 seconds. The water quality was regulated by running the system in low pressure for 30 minutes and experiments conducted with 15mg of gas per liter of water.

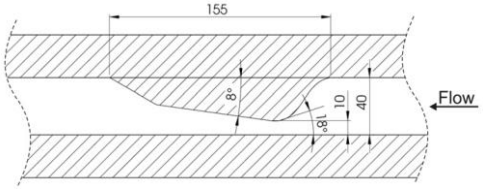

Figure 2 Venturi geometry and direction of flow

3 NUMERICAL SETUP

The dynamics of fluid flow through the venturi was simulated by using numerical approach. A CFD package, STAR-CCM+ finite volume stress solver, was used to solve governing equations (such as continuity and momentum) (SIEMENS PLM Software, 2016). Finite volume method discretises the integral formulation of the governing flow equations. The solver employs a predictor–corrector approach to link the continuity and momentum equations.

Detached eddy simulation (DES) is a hybrid modeling approach that combines features of Reynolds-Averaged (RANS) simulation in some parts of the flow and large eddy simulation (LES) in others based on predetermined flow property thresholds (Spalart et al., 1997).

DES turbulence models are set up so that boundary layers and irrotational flow regions are solved using a base RANS closure model. However, the turbulence model is intrinsically modified so that, if the grid is fine enough, it will emulate a basic LES subgrid scale model in detached flow regions. In this way, one gets the best of both worlds: a RANS simulation in the boundary layers and an LES simulation in the unsteady separated regions (SIEMENS PLM Software, 2016).

The setup of the DES necessitated determination of a number of crucial settings for the setup of the simulation. Within this framework, turbulence model selected in this study was a DES Version of the SST K-Omega Model (Menter & Kuntz, 2004). DES solver utilized a segregated flow model which solves the flow equation in an uncoupled manner. Convection terms in the DES formulations were discretized by applying a second-order upwind scheme. The overall solution obtained using Improved Delayed Detached Eddy Simulation (IDDES) of Shur et al., (2008).

Overall, with the mesh refinement and volumetric mesh enhancements, the domain was meshed with 3 million cells as in Figure 3. The computational domain used for the simulations is presented by Figure 4. Thus, inlet boundary was placed at the right hand side of the figure at 100mm distance and outlet was placed on the left hand side at 200mm away from the venturi throat. The venturi surface was defined as a non-slip wall and rest as slip wall.

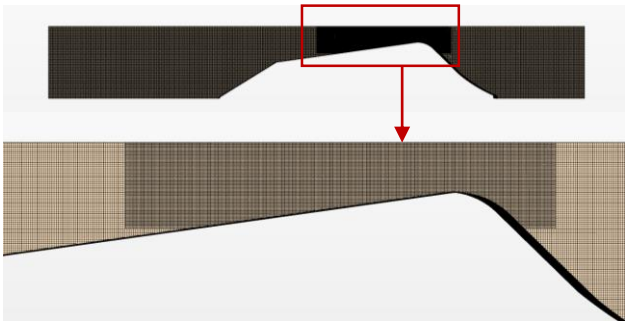

Figure 3 Volume mesh of the venturi with volumetric refinement

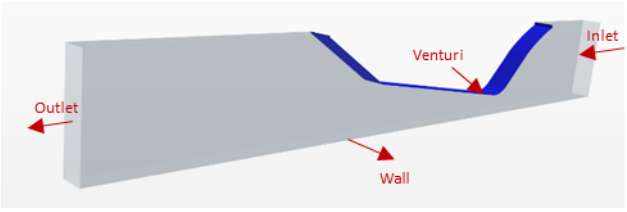

Figure 4 boundary conditions of the computational domain

The convective Courant number is used as an indicator to select the time-step size for the simulation (Courant et al., 1928). For time-accurate simulations, the convective Courant number set to be 1.0 on average within the whole domain with target maximum Courant number being 5. This value implies that the fluid moves by about one cell per time step. Minimum time step for the simulation was restricted to 1.6×10^{-5} s.

The cavitation models and the gas dissolution model in STAR-CCM+ are based on the Rayleigh–Plesset equation (Plesset & Prosperetti, 1977; Plesset, 1949). The full Rayleigh–Plesset model includes the influence of bubble growth acceleration, as well as viscous and surface tension effects. The bubble-growth velocity that is needed for the source term of the vapor volume fraction equation is computed without neglecting any of the terms in the Rayleigh-Plesset equation.

$$R\frac{\mathrm{d}v_r}{\mathrm{d}t}+\frac{3}{2}v_r^2=\frac{p_v-p}{\rho_l}-\frac{2\sigma}{\rho_l R}-4\frac{\mu_l}{\rho_l R}v_r \qquad (2)$$

where: $\frac{\mathrm{d}v_r}{\mathrm{d}t}$, is the substantial derivative of the bubble growth rate, σ is the surface tension, ρ_l is the liquid density.

The setup also adopted some reference parameters such as vapour pressure as P_v=3574 Pa, absolute pressure as P =454000Pa and reference speed as U=24.7m/s through the venturi throat following Jian et al. (2015). The established conditions corresponded to free stream cavitation number of 1.48 matching the experimental case. This is calculated using

$$N_{cav}=\frac{p-p_v}{\frac{1}{2}\rho_l U^2} \qquad (3)$$

where: U is the velocity.

Water quality properties measured by the experiments were also implemented by the CFD simulations. 15mg gas per liter was converted to seed diameter and number of nuclei per meter cube as $7.5*10^{-5}$m and $7*10^{7}$ respectively.

4 RESULTS

Following the appropriate setup of the simulations, to serve the main aim of the carried out study, cavitation observations and erosive indicators are compared with the experimental findings with a view to calibrate erosive indicator threshold values for propeller and rudder cases.

In order to make sure experimental case is resurrected appropriately both venturi throat average velocity and absolute pressure inlet were monitored. This ensured the accurate representation of cavitation phenomenon. Following this, erosive indicators discussed in the Introduction were implemented within the software environment. Thus, GLM, IFM and Erosive Power functions were employed for this purpose. In addition, those functions developed in house by LR were also employed.

It should be noted that in order to satisfy the Courant number being smaller than 1, the computational mesh should be very fine with a small time step. It suggests that total computational time is significant even for a model scale geometry. For example, it took 2 months to run the 1 sec real-time part of the case on 12 processor workstation of Strathclyde University. The convective CFL number introduced in STAR CCM+ v11.06 helped significantly to satisfy keeping the CFL number at an average of 1 for the overall domain and increasing the time step when possible.

Following Figure 5 presents the cavitation volume predicted by the simulation. An important remark about this figure is the chaotic fluctuation of the cavitation volume over time. This consequently means that the assumption of the repeatability of the cavitation events is not applicable for this kind of multiphase simulations.

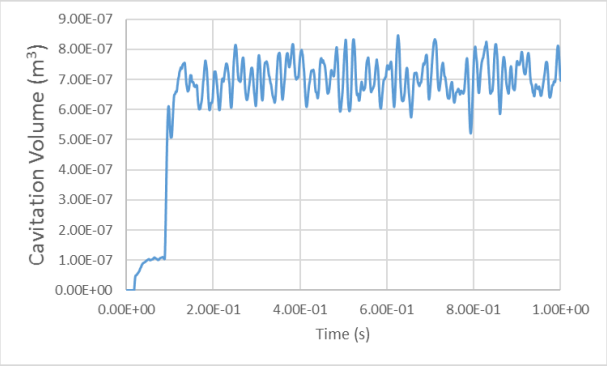

Figure 5 Cavitation volume report of the simulation

Figure 6 presents the cavitation observations during the experiment and compares them against the CFD simulations by LR and Strathclyde University. The cavitation predictions are plotted for iso surfaces corresponding to the value of 0.5 and iso surface range of 0.1 to 1 vapor volume fraction. It is apparent from the comparisons that cavitation simulations agree well with the experimental cavitation observations. Solution of full Rayleigh-Plesset equations observed to improve the accuracy of the cavitation simulations.

Based on the confidence gained through the comparisons of the experimental cavitation observations versus cavitation simulation predictions, further evaluations are conducted regarding the erosive indicators. Erosive indicators defined within the software were summed and averaged over time to compare against the experimental erosion extent.

As shown by Petkovšek & Dular (2013), the model test paint removal suggests there are two main erosion zones (top section of Figure 7 and 8). It is shown the first zone corresponds to the area where the main cavitation sheet collapse (denoted by 1) and the second where detached cavitation structures collapse (denoted by 2).

Figure 7 presents the comparisons conducted for the 1 second mark of the experiments for Erosive Power function, IFM and GLM as predicted by the numerical simulation. Initially, simulations results are plotted and scaled in order to match the experimental figures. Erosive Power function presented by part A in Figure 7 observed to show erosive indication in the 2nd region while the 1st region is performing poor with not much erosive indication. However, there is a concentration of light blue contour at the downstream edge of the 1st region. This shift in the location may be due to the time mismatch between the simulation and experiments. IFM presented by part B in Figure 7 shows a dense concentration in the 1st region while relatively small area of erosion is predicted in the 2nd region. Erosive indication by GLM is promising in terms of its appearance being similar to the experimental observations with scattered pitting look as shown in part C of Figure 7. Yet, erosive indication by GLM is more concentrated in the 1st region in comparison to the 2nd which does not agree with the experimental observations.

Erosion prediction done by LR (Figure 8) roughly shows the two zones, but functions appear as strips perpendicular to the flow. It can be also noted that the erosion prediction done by LR looks symmetrical along middle longitudinal line. This behavior was not noticed in the experiment and should not be predicted by fairly realistic DES model, so further investigation is required to clarify this finding. The functions utilized are developed in house by LR as previously reported in (Ponkratov, 2015; Ponkratov & Caldas, 2015) and showed good correlation on model and ship scale geometries.

Experiment	CFD (iso surface of vapour fraction 0.5)	CFD (iso surface of vapour fraction 0.1 to 1)
t_0		Solution Time 0.381987 (s)
$t_0+5\Delta t$		Solution Time 0.382787 (s)
$t_0+10\Delta t$		Solution Time 0.383587 (s)
$t_0+15\Delta t$		Solution Time 0.384387 (s)
$t_0+20\Delta t$		Solution Time 0.385187 (s)
$t_0+25\Delta t$		Solution Time 0.385987 (s)
$t_0+30\Delta t$		Solution Time 0.386787 (s)
$t_0+35\Delta t$		Solution Time 0.387587 (s)
$t_0+40\Delta t$		Solution Time 0.388387 (s)
$t_0+45\Delta t$		Solution Time 0.389187 (s)
$t_0+50\Delta t$		Solution Time 0.389987 (s)
$t_0+55\Delta t$		Solution Time 0.390787 (s)

Figure 6 Cavitation structure evolution recorded during the test (left column) and CFD predictions for iso surface of 0.5 vapour volume fraction (middle column) and simulation results for iso surface range of 0.1 to 1 (Right column). CFD pictures are presented with time intervals corresponding to model test ones.

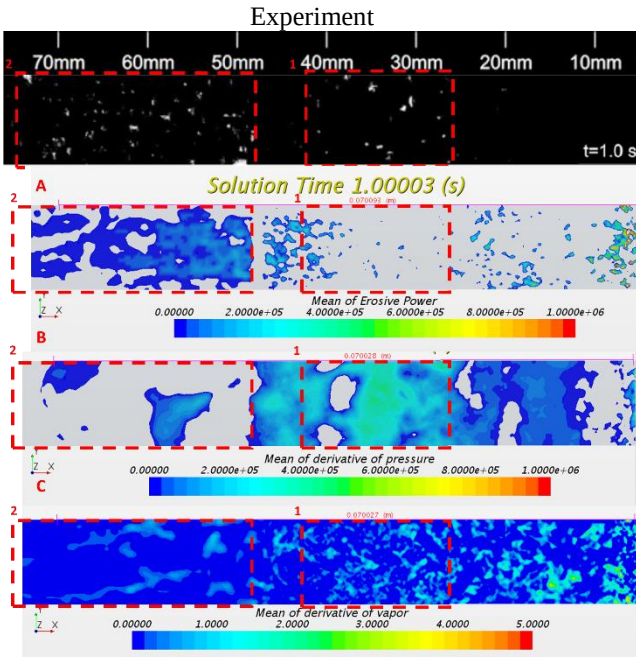

Figure 7 Experimental and CFD indication of cavitation erosion at 1 second using Erosive Power function (A), IFM (B) and GLM (C).

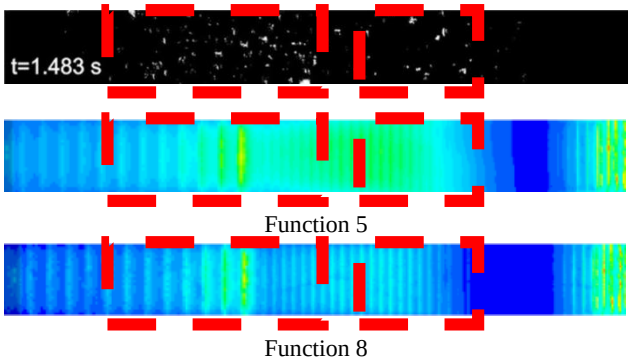

Figure 8 Experimental and CFD (Functions 5 and 8) indication of cavitation erosion.

Based on the observations and comparisons of the erosive indicators against the experimental findings, it is concluded that best performing method for this particular case is the Erosive Power function. The threshold of the contour that has been set for the best comparison can now be utilized for a more conventional marine application. An exemplary application can be made to that propeller of Usta et al. (2017) based on the experiments conducted by (Mantzaris et al., 2015) as shown by Figure 9.

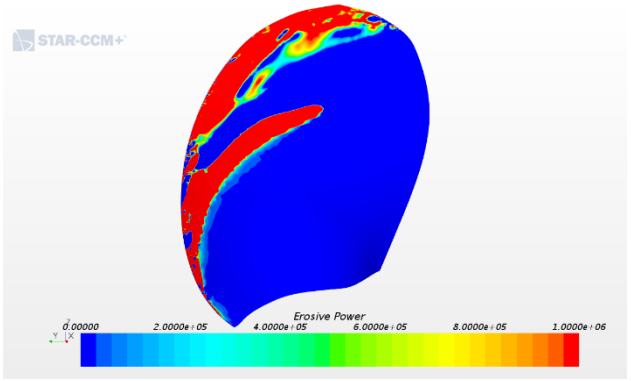

Figure 9 Calibrated Erosive Power threshold applied to propeller simulation conducted by Usta et Al. (2017).

The calibrated threshold predictions show reasonable agreement when compared with observations made by Mantzaris et al., (2015). The erosion is observed to take place where light blue color is present from the results of Petkovšek & Dular (2013). If light blue color is assumed to be an indicator, then erosion is predicted in mic-chord to trailing edge region of the 0.7 r/R of the propeller which is also shown soft paint removal as an indicator of erosion in Figure 10.

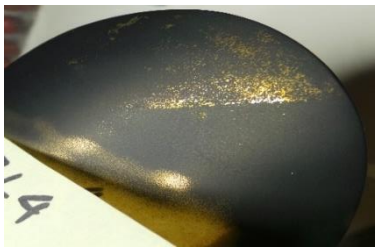

Figure 10 Experimental cavitation erosion tests by Mantzaris et al., (2015).

5 CONCLUSION

This study presents a time accurate numerical cavitation erosion prediction based on the experimental study conducted by Petkovšek & Dular (2013) that achieved visual cavitation erosion within 1.5 seconds. The simulation setup incorporates state of the art computational options such as full Rayleigh-Plesset equation solution and convective CFL number selection.

The comparisons of the cavitation observation between the experimental studies and CFD simulation results shown satisfactory resemblance despite the presence of highly dynamic cavitation phenomenon. The implemented erosive indicators IFM and GLM predictions for the first 1 second duration did not show encouraging results when compared against the experimental observations. However, Erosive Power function predictions observed to perform relatively better. The Erosive Power threshold values are then utilized to calibrate the erosive thresholds on a propeller.

The erosive indicators implemented by the LR is found to indicate two domains with erosion concentration with some shift along the downstream of the flow which is also observed by the experimental findings. Yet, LR predictions have little resemblance of the experimental pitting as experiments showed scattered dots like appearance whilst LR functions showed 2D strips. This will be investigated further.

Overall, whilst the case at first looks like a simple setup, due to dynamic cavitation and significant venturi throat contraction ratio, there exists some severe cavitation dynamics such as rebounding, separation and bursting. By simulating this case, a time accurate Erosive Power function threshold calibration is applied to a propeller with reasonable success. Yet, more established erosion prediction functions, such as IFM and GLM and Function 5 and 8 by LR, which worked well on more complex geometries such as propellers, foils and rudders, did not

perform as expected for this particular case. The deviations experienced by these erosive indicators need careful care and scrutinization to better understand the origin of these discrepancies. At this point, it is unclear whether the discrepancies are due to CFD codes or to algebraic nature of the empirical erosive indicators. Systematic validation efforts are required in order to assess the validity of the CFD codes and the erosive indicators for predicting cavitation erosion tendency.

REFERENCES

Bark, G., & Bensow, R. E. (2014). Hydrodynamic processes controlling cavitation erosion. *Fluid Mechanics and Its Applications*, ***106***, pp.185–220.

Bark, G., Berchiche, N., & Grekula., M. (2004). "Application of Principles for Observation and Analysis of Eroding Cavitation-The EROCAV Observation Handbook. *EROCAV Report, Dept. of Naval Architecture, Chalmers University of Technology, Göteborg, Sweden*.

Courant, K., Friedrichs, R., & Lewyt, H. (1928). On the Partial Difference Equations of Mathematical Physics. *Mathematische Annalen*, ***100,*** pp.32–74.

Dular, M., Stoffel, B., & Širok, B. (2006). Development of a cavitation erosion model. *Wear*, ***261***(5–6), pp.642–655.

Eskilsson, C., & Bensow, R. E. (2015). Estimation of Cavitation Erosion Intensity Using CFD: Numerical Comparison of Three Different Methods. *4th International Symposium on Marine Propulsors (smp'15)*, (June).

Jian, W., Petkovšek, M., Houlin, L., Širok, B., & Dular, M. (2015). Combined Numerical and Experimental Investigation of the Cavitation Erosion Process. *Journal of Fluids Engineering*, ***137***(5), pp.51302.

Mantzaris, A., Aktas, B., Fitzsimmons, P., & Atlar, M. (2015). Establishment and verification of reproducible method for coating propeller blades for erosive cavitation detection. In *The 4th International Conference on Advanced Model Measurement Technologies for the Maritime Industry*. Istanbul, Turkey.

Menter, F., & Kuntz, M. (2004). Adaptation of eddy-viscosity turbulence models to un- steady separated flow behind vehicles. *The Aerodynamics of Heavy Vehicles: Trucks, Buses, and Trains*, ***19***, pp.339–352.

Petkovšek, M., & Dular, M. (2013). Simultaneous observation of cavitation structures and cavitation erosion. *Wear*, ***300***(1–2), pp.55–64.

Plesset, M. S. (1949). The dynamics of cavitation bubbles. *Journal of Applied Mechanics*, ***16***(3), pp.277–282.

Plesset, M. S., & Prosperetti, a. (1977). Bubble Dynamics and Cavitation. *Annual Review of Fluid Mechanics*, ***9***(1), pp.145–185.

Ponkratov, D. (2015). DES Prediction of Cavitation Erosion and Its Validation for a Ship Scale Propeller. *Journal of Physics: Conference Series*.

Ponkratov, D., & Caldas, A. (2015). Prediction of Cavitation Erosion by Detached Eddy Simulation (DES) and its Validation against Model and Ship Scale Results. *Fourth International Symposium on Marine Propulsors (SMP)*.

Shur, M. L., Spalart, P. R., Strelets, M. K., & Travin, A. K. (2008). A hybrid RANS-LES approach with delayed-DES and wall-modelled LES capabilities. *International Journal of Heat and Fluid Flow*, ***29***(6), pp.1638–1649.

SIEMENS PLM Software. (2016). STAR-CCM+ User Guide Version 11.06.

Spalart, P. R., Jou, W. H., Strelets, M., & Allmaras, S. R. (1997). Comments on the feasibility of LES for wings and on a hybrid RANS/LES approach. *Advances in DNS/LES*.

Usta, O., Aktas, B., Maasch, M., Turan, O., Atlar, M., & Korkut, E. (2017). A study on the numerical prediction of cavitation erosion for propellers. *Fifth International Symposium on Marine Propulsion, SMP'17*, ***Helsinki,F***(June).

van Terwisga, T. J. C., Fitzsimmons, P. A., Ziru, L., & Foeth, E. J. (2009). Cavitation Erosion – A review of physical mechanisms and erosion risk models. *Proceedings of the 7th International Symposium on Cavitation*, (41), pp.1–13.